

DEPARTMENT OF THEORETICAL PHYSICS AND COMPUTER MODELLING

Head of Department *Dr. hab. phys.* Eugene Kotomin

Research Area and Main Problems

Our theoretical research interests are focused on six classes of problems related to:

- kinetics of diffusion-controlled processes, with emphasis on pattern formation and catalytic surface reactions;
- the atomic and electronic structure of numerous advanced materials, with emphasis on calculations of properties of defects, surfaces, metal/insulator interfaces.
- theoretical simulations and experimental studies of nanostructures and nanomaterials;
- modeling of advanced functional materials for energy applications (fuel cells, ceramic membranes, Li batteries, fusion and fission reactors);
- stochastization of magnetic field lines in magnetized fusion plasma;
- gyrotron development for thermonuclear reactors .

We combine several different techniques, including analytical formalisms and large-scale computer simulations (quantum chemical methods, stochastic simulations as well as Monte Carlo/cellular automata modeling)—for more details see our homepage <http://www1.cfi.lu.lv/teor>

Staff

Laboratory of kinetics in self-organizing systems	Laboratory of computer modeling of electronic structure of solids
Dr. O. Dumbrajs	B.Sc. J. Begens
Dr. D. Gryaznov	Dr. D. Bocharov
Dr. V. Kashcheyevs	Dr. R. Eglitis
Dr. E. Klotins	M.Sc. A. Gopejenko
Dr. hab. E. Kotomin	B.Sc. J. Kazerozskis
Dr.hab. V. Kuzovkov	B.Sc. O. Lisovski
M.Sc. P. Merzljakovs	Dr. Yu. Mastrikov
Dr. A. Popov	Dr. S. Piskunov
M.Sc. J. Shirmane	Dr. hab. Yu. Shunin
Dr. G. Zvejnieks	M.Sc. A. Sorokin
	Dr. Yu. Zhukovskii

Scientific visits abroad

1. Dr. hab. E. Kotomin, Max-Planck Institut für Festkörperforschung, Stuttgart, Germany (9 months), Eurasian National University, Astana, Kazakhstan (2 weeks)
2. Dr. O. Dumbrajs, Karlsruhe Institute of technology (KIT) , Germany (7 weeks)
3. Dr. D. Gryaznov, Max-Planck Institut für Festkörperforschung, Stuttgart, Germany (9 months)
4. Dr hab. V. Kuzovkov, Northwestern University, Evanston, Illinois, USA (3 months)
5. Dr. A. Popov, Laue-Langevin Institute, Grenoble, France (1 month); Institute of Materials Science, Darmstadt University of Technology, Germany (5 weeks); Institute of Physics, University of Tartu, Estonia (2 weeks)
6. M.Sc. A. Sorokin, Technical University of Berlin, Germany (4.5 months)
7. M.Sc. A. Gopejenko, Institute for Applied Materials, Karlsruhe Institute of Technology Karlsruhe, Germany (3 months)
8. B.Sc. O. Lisovski, Uppsala University, Sweden (10 months)
9. B.Sc. J. Kazerovskis, University of Ulm, Germany (3.5 months)
10. Dr. Yu. Mastrikov, Institute of Applied Materials, Karlsruhe, Germany (1 month), Eurasian National University, Astana, Kazakhstan (2 weeks)
11. Dr. S. Piskunov, Laboratori Nazionali di Frascati, Italy (2.5 months); University of Duisburg-Essen, Germany (2 months), Institute of General and Inorganic Chemistry, Moscow, Russia (1 month)
12. Dr. hab. Yu. Shunin, Laboratori Nazionali di Frascati, Italy (5 weeks); Institute of Nuclear Problems, Belorussian State University, Minsk, Belarus (1 week)
13. Dr. Yu. Zhukovskii, St. Petersburg State University, Russia (1 month), Institute of Applied Materials, Karlsruhe, Germany (1 month)

International Cooperation

Belarus	1. Institute of Nuclear Problems, Belarussian State University, Minsk (Prof. S.A. Maksimenko)
Estonia	2. Institute of Physics, University of Tartu (Prof. A. Lushchik)
Finland	3. Helsinki University of Technology (Dr. T. Kurki-Suonio)
France	4. Laue-Langevin Institute, Grenoble (Dr. G.J. McIntyre, Dr. H. Schober)
Germany	5. Max Planck Institut für Festkörperforschung, Stuttgart (Prof. Dr. J. Maier)
	6. Deutsches Elektronen-Synchrotron DESY, Hamburg (Dr. A. Kotlov)
	7. Darmstadt University of Technology, Darmstadt (Dr. J. Zimmermann)
	8. Max Planck Institut für Plasmaphysik, Garching (Dr. V. Igochine, Prof. Dr. K. Lackner, Dr. R. Mayer-Spasche, Prof. Dr. H. Zohm)
	9. Institut für Hochleistungsimpuls & Mikrowellentechnik (KIT), Karlsruhe (Drs. S. Kern, B. Piosczyk)
	10. Institut für Angewandte Materialien (KIT), Karlsruhe (Drs. A. Möslang, P. Vladimirov)
	11. Department of Theoretical Chemistry, University of Duisburg-Essen, (Prof. E. Spohr)

Greece	12. School of Electrical and Computer Engineering, National Technical University of Athens, Zographou (Dr. K. Avramides)
Israel	13. Ben Gurion University, Beer Sheeva (Prof. A. Aharony, Prof. D. Fuks)
Italy	14. Laboratori Nazionali di Frascati (Rome) (Dr. S. Bellucci, Dr. M. Cestelli-Guidi)
Kazakhstan	15. Gumilyov National University, Astana (Prof. A. Akilbekov)
Japan	16. FIR Center, University of Fukui (Prof. T. Idehara)
Lithuania	17. Institute of Semiconductor Physics (SPI), Vilnius (Dr. E. Tornau)
Poland	18. Warsaw University, Dept of Chemistry (Dr A. Huczko)
Romania	19. University of Craiova (Dr. D. Constantinescu)
Russia	20. St. Petersburg State University (Prof. R.A. Evarestov) 21. Institute of General and Inorganic Chemistry, Russian Academy of Sciences, Moscow (Prof. P.N. Dyachkov)
UK	22. University College London (Prof. A.L. Shluger)
Ukraine	23. National University, Lviv (Prof. I. Bolesta, Drs. I. Karbovnyk, V. Lesivtsiv, S. Velgosh and I. Rovetsky) 24. Institute for Scintillator Materials, Kharkov (Prof. A. Gektin)
USA	25. Northwestern University, Evanston, Illinois (Prof. M. Olvera de la Cruz) 26. University of Maryland, College Park (Dr. G.S. Nusinovich, Dr. M.M. Kuklja) 27. Lawrence Berkeley National Laboratory, Berkeley, California (Dr. G.A. Bizarri) 28. Wake Forest University, Winston-Salem, North Carolina (Prof. R.T. Williams)

Main Results

A. Electronic structure calculations for advanced materials

ELECTRONIC AND THERMODYNAMIC PROPERTIES OF WURTZITE-TYPE ZnO CRYSTAL CONTAINING OXYGEN VACANCIES OR IMPURITY ATOMS AND Al_{Zn} SUBSTITUTE ATOMS

D. Gryaznov, A. Sorokin, E.A. Kotomin, Yu.F. Zhukovskii, J. Purans

R.A. Evarestov,

Department of Quantum Chemistry, St. Petersburg State University, Russia

A. Bussmann-Holder, J. Maier

Max Planck Institute for Solid State Research, Stuttgart, Germany

Our *ab initio* LCAO calculations performed using the hybrid PBE0 exchange correlation functional (with the standard HF exact exchange contribution of 0.25) show good agreement of the electronic and phonon properties of V_O-containing wurtzite-type ZnO crystal (Fig. 1) with the corresponding experimental results. The calculated Raman- and infrared-active phonon frequencies in defect-free hexagonal ZnO were found to be in a

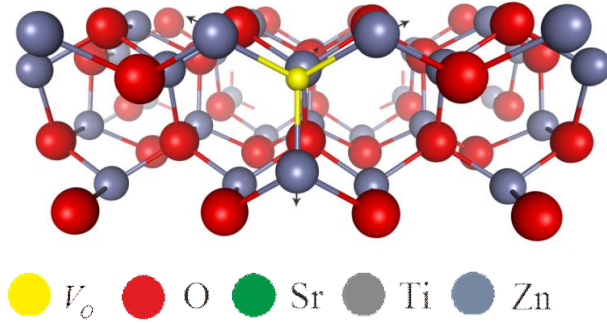


Figure 1. The atomic structure of wurtzite-type ZnO containing a single oxygen vacancy. O and Zn atoms as well as V_O vacancy are shown as large red, middle gray-blue and small yellow balls. The arrows show the relaxation pattern around V_O .

good agreement with experimental results. The additional “ghost” basis set centered at the vacancy site considerably affects the defect formation energies and leads to the pattern of almost singly ionized oxygen vacancies (one electron trapped in/around the vacancy). The corresponding defect formation energy in w -ZnO at 0 K (4.20 eV) is well converged with respect to the supercell size and its value is consistent with the experiments. The temperature dependences of the Gibbs free energies for formation of O vacancies in w -ZnO depending on their concentration were calculated taking into account the phonon contribution (Fig. 2). The temperature dependence of the soft modes as calculated for a

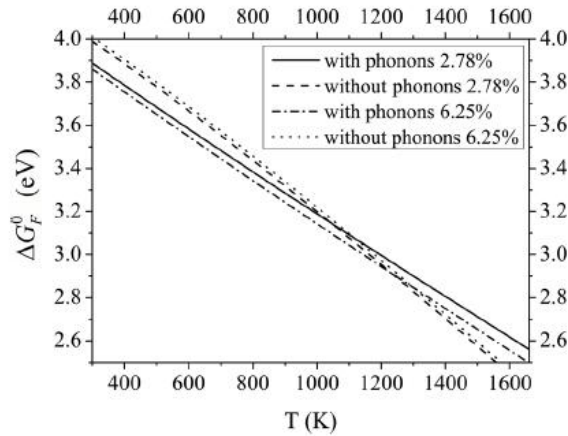


Figure 2. The calculated Gibbs free energy (*per* vacancy) of formation of oxygen vacancy (ΔG_F^0) with and without phonon contribution in the solid phase as a function of temperature in w -ZnO. The inset shows different defect concentrations for both cases. The distances between V_O vacancies in ZnO are 6.52 and 9.78 Å for 6.25% and 2.78%, respectively.

defect-free w -ZnO within the polarizability model is of key importance for the correct calculation of the defect formation energy. Supercell finite-size effects on values of ΔG_F^0 are caused by a considerable localization of electronic density around V_O vacancy in w -ZnO.

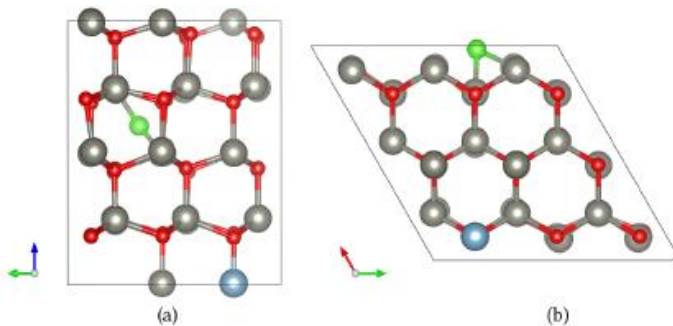


Figure 3. Images of w -ZnO:Al structure containing O_i impurity atom along $[\bar{1}00]$ (a) and $[00\bar{1}]$ (b) axes: 73-atom supercell containing 35 Zn_{Zn} (large grey), 36 O_O (small red), 1 Al_{Zn} (large blue) un 1 O_i (middle green) atoms.

In absence of interstitial O_i atoms, group IIIA metal- (especially Al-) doped ZnO (ZA) exhibits a low resistivity while retaining a high optical transparency, thus, being a prominent material for optoelectronics. However, these properties may be destroyed even with small concentrations of oxygen-related defects (*e.g.*, O_i atoms, such a structure is designated as ZAO). This difference can be illustrated by comparison of band structures and DOS for ZA and ZAO (Fig. 4).

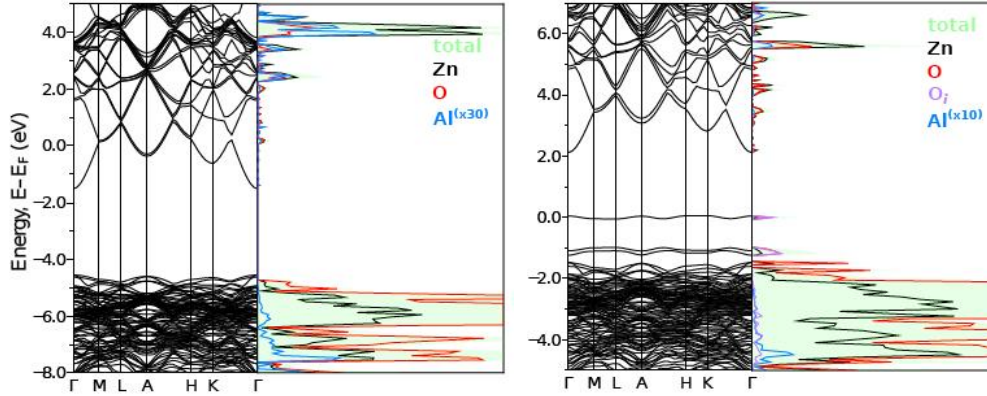


Figure 4. The band structure and DOS of ZA and ZAO (left/right panels, resp.) for 72-atom supercells.

Obviously, for ZA there is no distinct defect level as Al states are mixed with ZnO bands. However, the Fermi level crosses conduction bands, therefore, introducing Al substitute into *w*-ZnO induces the insulator-to-metal transition. On the contrary, in the case of ZAO, there are three distinct defect levels appear in the band structure and DOS, all of which consist mainly from O_i contributions. Al states, on the contrary, are delocalized over valence and conductivity bands as in ZnO:Al. Positions of O_i levels make defective ZAO structure an electron acceptor.

FIRST PRINCIPLES SIMULATIONS OF HYDROGEN IMPURITIES IN ZnO BULK AND ON ZnO(10 $\bar{1}$ 0) SURFACE

E.A. Kotomin, Yu.F. Zhukovskii, A. Sorokin, J. Purans

A. Usseinov, A.T. Akilbekov

L. N. Gumilyov Eurasian National University, Kazakhstan

Hydrogen atoms unavoidably incorporated from plasma during growth of ZnO considerably affect their electrical conductivity. Supercell models of single hydrogen atom incorporated in the bulk and upon the non-polar ZnO (10 $\bar{1}$ 0) surface were calculated using hybrid LCAO method. The incorporation energy, the atomic relaxation, the electronic density redistribution and the electronic structure modifications were compared for both bulk interstitial H position (Fig. 5) and the surface adsorption (Fig. 6). It has been shown that hydrogen has a strong binding with the nearest bulk and surface O ions characterized by incorporation energy of the former *per* 2 \times 2 \times 2 supercell (1.8 eV) and adsorption energy of the latter *per* 2 \times 2 surface supercell. Obviously, incorporation of H_i atom into the bulk is energetically unfavorable.

The energetically most favorable position of H_i atom in *w*-ZnO bulk has been found to be the interstitial site near the oxygen atom in a regular lattice, the so-called anti-bonding (AB) configuration perpendicular to *c* axis (Fig. 5). Analogously, the most preferable

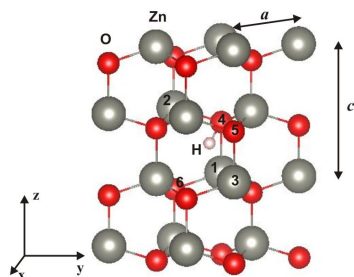


Figure 5. Structural model of the w -ZnO ($2 \times 2 \times 2$) supercell containing the hydrogen impurity atom (H_i). Enumerated Zn and O atoms are the nearest neighbors of H_i being relaxed around it.

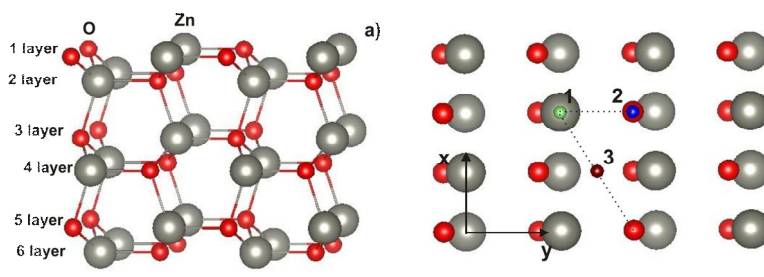


Figure 6. Unrelaxed 6-layer slab model of the ZnO($10\bar{1}0$) surface (a) and top view of the three possible different positions for the adsorption of hydrogen atom upon it (b): 1 – atop surface Zn atom, 2 – atop surface O atom, 3 – hollow position for H adatom. In the case of the lowest H adatom concentration, ZnO (2×2) surface supercell has been constructed.

adsorption position of H atom upon ZnO($10\bar{1}0$) surface has been found to be site 2 atop the surface O atom (Fig. 6). Comparative analysis of the electronic structure of ZnO:H bulk and H/ZnO($10\bar{1}0$) interface confirms that hydrogen atom in both cases is anti-bonding, moreover, it is a shallow donor. Therefore, we would expect a high concentration H nearby ZnO surfaces could make a considerable contribution to the electronic conductivity (surface metallization).

AB INITIO CALCULATIONS OF POINT DEFECTS IN INORGANIC NANOTUBES (BN, SrTiO₃, TiO₂ NANOTUBES CONTAINING SUBSTITUTE DEFECTS)

S. Piskunov, Yu.F. Zhukovskii, S. Lisovski, J. Kazerovskis, J. Begens

P.N. D'yachkov, D.V. Makaev

Kurnakov Institute of General and Inorganic Chemistry, Russian Academy of Sciences, Moscow, Russia

E. Spohr

Department of Theoretical Chemistry, University of Duisburg-Essen, Germany

S. Bellucci

INFN-Laboratori Nazionali di Frascati, Frascati (Rome), Italy

Inorganic nanotubes (NTs) are important and widespread materials in modern nanotechnology. Moreover, imperfect NTs with reproducible distribution of point defects attract enhanced interest, due to potential production of novel innovative nanomaterials and devices. A variety of experimental conditions accompanying their synthesis can certainly promote the appearance of point defects: native vacancies or antisites as well as substitutional impurities. These and other types of irregularities may occur in inorganic NTs as a result of the growth process or intentionally induced to modify their properties. Point defects also play the role of chemically active sites for NT-wall functionalization. This study analyzes a series of results obtained using *ab initio* simulations on both perfect and defective BN NTs, TiO₂ NTs as well as SrTiO₃ NTs.

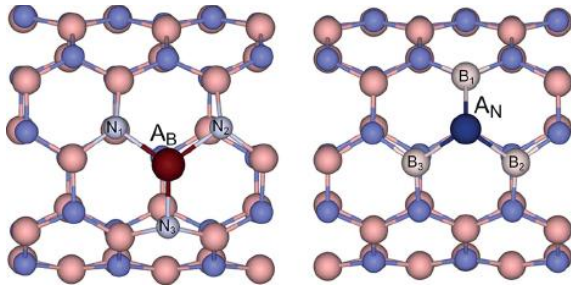


Figure 7. Schematic representation of substitutional defect-containing BN NT (A_h /BN NT) unit cells as calculated using the PBE0-LCAO method with the total geometry optimization: A_B /BN NT (left panel) where A_h are Al, Ga and In; A_N /BN NT (right panel) where A_h are P, As and Sb. N atoms are shown as blue (dark) balls, while B atoms are shown as pink ones.

Using hybrid exchange–correlation functionals applied within the density functional theory (DFT), the following extrinsic isoelectronic substitutional impurities in BN NTs (Fig.7) have been calculated: Al_B , P_N , Ga_B , As_N , In_B , and Sb_N as they may produce a strong effect in the luminescence spectra of nanostructured BN.

Extrinsic substitutional impurities in the TiO_2 NTS and $SrTiO_3$ NTs (Fig. 8) for further *ab initio* calculations have been chosen C_O , N_O , S_O , and Fe_{Ti} since they essentially enhance photocatalytic activity of both nanotube types. The calculated variations in the formation energies

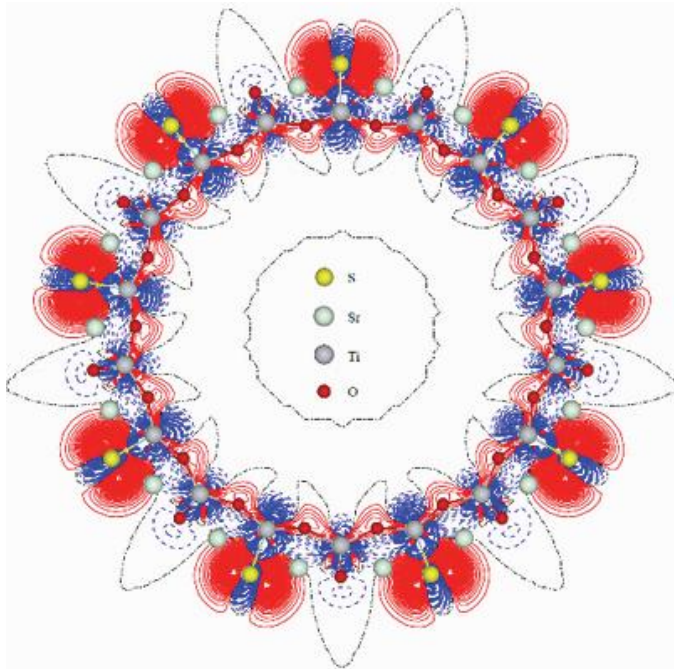


Figure 8. 2D difference electron-density plots projected onto the section planes across $SrTiO_3$ nanotube containing an impurity defect C_O / $SrTiO_3$ NT. Ti are shown as gray balls, O as red (dark gray) balls, Sr as green (gray), substitution impurity atoms (A_h) are shown in yellow (light gray). Atoms that are positioned outside the crossing plane are shown in dimmed colors. Dash-dotted (black online) isolines correspond to the zero level. Solid (red) and dashed (blue) isolines describe positive and negative values of the difference in electron density, respectively.

obtained for equilibrium defective nanostructures allow one to predict the most stable compositions, irrespective of the changes in growth conditions. Calculated charge–density maps (Fig. 8) of the different tubular nanostructures containing extrinsic substitutional impurity atoms highlighted changes in the charge distribution caused by doping. This means that the increased covalency in defect–host atom bonds may lead to an enhancement of adsorption properties. This would imply that defective NTs can be used in gas-sensing devices. On the basis of the performed first-principles calculations, one may conclude that the presence of isoelectronic impurities significantly affects the band structure of the NTs under study, which must be taken into account when constructing nanoelectronic devices based on these NTs. All the mentioned effects can be observed by optical and

photoelectron spectroscopy methods, as well as by measuring the electrical properties of the NTs. Midgap levels positioned inside the optical bandgap of defective NTs make them attractive for band gap engineering in, for example, photocatalytic applications.

FORMATION OF Ni NANOCHAINS INSIDE CARBON NANOTUBES: FIRST PRINCIPLES SIMULATIONS

S. Piskunov, Yu.F. Zhukovskii, J. Kazerovskis

P.N. D'yachkov

Kurnakov Institute of General and Inorganic Chemistry, Russian Academy of Sciences, Moscow, Russia

S. Bellucci

INFN-Laboratori Nazionali di Frascati, Frascati (Rome), Italy

Carbon nanotubes with encapsulated monoatomic nanochains of magnetic metals (*e.g.*, Ni) are technologically important one-dimensional (1D) Me@CNT nanostructures fabricated and studied during recent years. Their mechanical, physical and chemical properties can be applied in various nanodevices as well as magnetic data storage and drug delivery platforms. In addition, the CNT walls can provide an effective barrier against oxidation and, thus, ensure long-term stability of the encapsulated metals. Nevertheless, the nanotubes filled with magnetic metals do not always display designed properties because the amount and location of magnetic particles inside the tubes are difficult to be controlled. To guide reliable fabrication of Me@CNT, it is important to understand the formation mechanism of metal nanochains or separated nanoparticles in nanotubes. Monoatomic chains of nickel atoms encapsulated into single-walled (SW) CNTs of armchair-type (n,n), $n = 3; 4; 5; 6; 7$ (Fig. 9a) and zigzag-type ($n,0$), $n = 7; 8; 9; 10; 11$ (Fig. 9b) chiralities have been considered in this study.

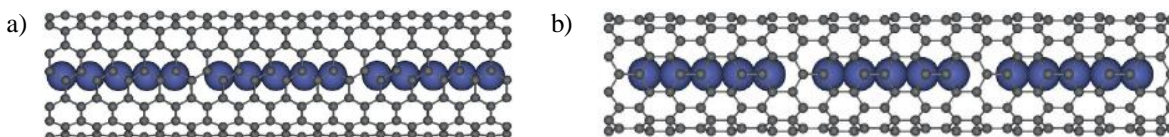


Figure 9. Schematic representation of selected equilibrium structures of Ni nanofilament inside (a) *ac*-CNT (7,7) and (b) *zz*-CNT (10,0) as calculated using PBE functional within the DFT-LCAO formalism. Small gray balls stand for carbon atoms, while large blue (dark gray) ones for nickel atoms.

Nanofilament encapsulation inside CNTs with diameter less than 6 Å (*i.e.*, (5,5) and (7,0) nanotubes of *ac*- and *zz*-chiralities) has been found energetically more favorable, due to stronger interatomic Ni–C bonding, while weakening of Ni–C bond of Ni@CNTs with diameter larger than 6 Å yields an additional freedom for formation of stronger Ni–Ni bonds leading to clusterization of Ni nanofilament (Fig. 9). In all the cases, monoatomic Ni nanochain preserves a ferromagnetic ground state with magnetic moment on Ni as twice as larger than in the Ni bulk (0.62 μB). Enhanced magnetic properties arise mainly from geometry dependent unfilled *d* band and *sp*–*d* hybridization effects typical for transition metal nanofilaments encapsulated inside nanotubes. Carbon nanotubes containing monoatomic Ni nanochains exhibit metallic behavior, even if pristine nanotube is semiconductor (*i.e.*, ($n,0$) CNTs). Therefore, encapsulation of Ni nanofilament in CNTs is a way to create the highly conductive 1D hybrid nanostructures suitable as interconnects for future nanoelectronic circuits.

ELECTROMAGNETIC PROPERTIES OF CARBON NANOTUBES AND GRAPHENE NANOLAYERS BASED NANOSTRUCTURES FOR NANOSENSOR SYSTEMS

Yu.N. Shunin, Yu.F. Zhukovskii

V.I. Gopeyenko, N.Yu. Burlutskaya, T.D. Lobanova--Shunina
Information Systems Management Institute, Riga, Latvia

S. Bellucci
INFN-Laboratori Nazionali di Frascati, Frascati, Italy

Fundamental electromagnetic properties of carbon nanotubes (CNTs) and graphene nanoribbons (GNRs) with the essential concentration of ‘dangling bonds’ as well as point defects and functionalized atomic groups of various concentrations are very sensitive to local external perturbations. The induced changes of local electronic density of states lead

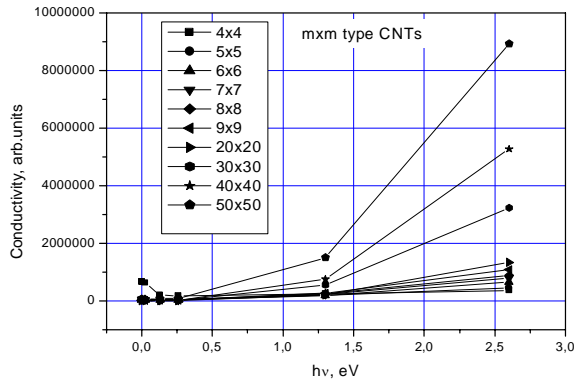


Figure 10. Conductivities of perfect *armchair* SW CNTs of various morphologies. *Note:* The critical frequency of about 0.25 eV corresponds to 60 THz

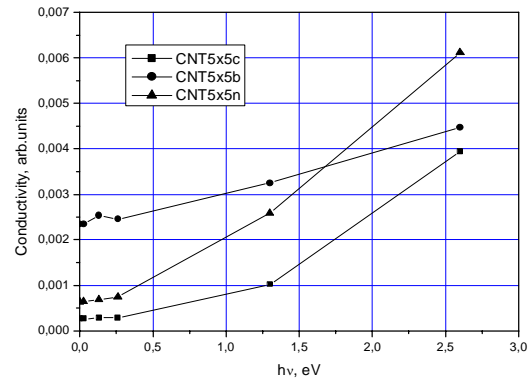


Figure 11. Conductivities of pure perfect and doped (B or N) CNTs in the limit of non-interacting defects.

to the correlated changes of current and spin states. The cluster approach based on the multiple scattering theory combined with effective medium approximation were used to the corresponding model including the dispersion law, electronic density of states, conductivity, *etc.* Multiple scattering problems were solved for nanostructures with radial and axial symmetry. Parametrical numerical simulations of conductivity using the formalism of Kubo-Greenwood were carried out for *zig-zag* $(m,0)$, *arm-chair* (m,m) and *chiral* (m,n) CNTs and GNRs. The sensitivity of their conductivity to the local electronic density of states with local impurities (N and B atoms) was demonstrated (Figs. 10 and 11). Both pure CNTs as well as 1D interconnects (CNT-Me and GNR-Me based nanostructures) were found to be fitting for applications in prospective nanosensor devices.

CNT-Fe-Pt INTERCONNECT ELECTROMAGNETIC SIMULATIONS OF MAGNETICALLY STIMULATED CNT GROWTH AS APPLIED FOR NOVEL MEMORY NANODEVICES

Yu.N. Shunin, Yu.F. Zhukovskii,

V.I. Gopeyenko, N.Yu. Burlutskaya, T.D. Lobanova--Shunina
Information Systems Management Institute, Riga, Latvia

S. Bellucci, F. Micciula
INFN-Laboratori Nazionali di Frascati, Frascati, Italy

The parametrically controlled production of carbon nanotubes (CNTs) with predefined morphologies is a topical technological problem for modern nanoelectronics. The chemical vapor deposition (CVD) technique for single walled carbon nanotubes (SW CNTs) in the presence of various metal nanoparticle catalysts is generally used now. The application of a magnetically stimulated CVD process scheme and catalyst nanoparticles with a strong magnetism promises additional possibilities for the CVD process management and allows expecting a predictable growth of CNTs with set chiralities and diameters. The main attention is focused on the Pt-Fe nanoparticles effect research. The developed cluster approach based on the multiple scattering theory formalism, realistic analytical and coherent potentials, as well as effective medium approximation (EMA-CPA), can be effectively used for modeling of nanosized systems. It allows us to calculate the dispersion law $E(\mathbf{k})$, electronic density of states, conductivity, *etc.* This theoretical approach is used

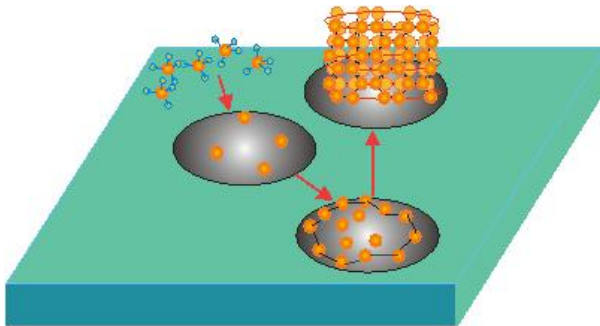


Figure 12. A model of the CVD process of CNT growth upon the catalytic nanoparticle surfaces

in simulations of fundamental electromagnetic properties in Pt-Fe-CNT interconnects, which are responsible for developing CNTs morphologies. The developed model of ‘effective bonds’ and the model of magnetic stimulation for growing CNTs morphologies generated on the Pt-Fe nanoparticle surface are applied for the evaluation of the expected CNT chiralities distribution. The model and conditions controlled magnetically, which stimulate CNT growth in the CVD process, aimed at the predictable SW CNT diameter and chirality and based on Pt-Fe catalyst are discussed. The possibilities of CNT bundle growth upon Fe-Pt nanoparticles for magnetic nanomemory devices are also evaluated.

The formation of the initial optimal perimeter for C-Metal (Fe-Pt) bonds is a synergetic process with a minimal free energy (Fig. 12). The nanoparticle diameter determines with a certain error the diameter of a CNT. The number of effective bonds defines the morphology of the future CNT in terms of growing nanotube chirality. Obviously, there is a considerable uncertainty in CNT morphology, owing to sporadic thermal dynamics of the deposited carbon atoms.

QUANTUM CHEMISTRY CALCULATIONS ON ScF₃ ELECTRONIC STRUCTURE AND LATTICE DYNAMICS

D. Bocharov, S. Piskunov, P. Zhgun, A. Kuzmin, J. Purans

ScF₃ is a perovskite-type material with a cubic ReO₃-type structure (space group Pm-3m). Recently it was found that ScF₃ undergoes strong negative thermal expansion (NTE) over a wide range of temperatures from 10 to 1100 K. In the current activity ScF₃ electronic structure, lattice dynamics, and phonon anharmonicity were studied within the framework of quantum chemistry approaches (LCAO, HF-DFT) using Crystal09 program. Electronic structure of ScF₃ (band structure, DOS, Mulliken analysis) are calculated for the first time. This study predicts that Sc-F bond has considerable covalent nature, F 2*p* and Sc 3*d* states are hybridized. The band gap obtained in HF-DFT calculations is equal to 8-10 eV and is in excellent agreement with those experimentally observed.

It has been found, that Sc position in the middle of regular ScF₆ octahedron is stable. Grüneisen parameters are calculated and phonon mode anharmonicity are studied in the Γ , X , M , R points of the Brillouin zone. It has been found that all modes investigated are harmonic except soft modes in R and M points. Grüneisen parameters of soft modes and coefficients describing mode's anharmonic potentials are found to be strongly dependent upon calculation technique used. Simple model that accounts static lattice energy and contribution of oscillator (R soft mode) is capable to describe NTE at low temperatures. This suggests that NTE occurs due to R and M mode softness.

THEORETICAL AND EXPERIMENTAL MODELING OF MATERIALS FOR RESISTIVE SWITCHING MEMORIES

E.A. Kotomin, D. Gryaznov, A. Kuzmin, J. Purans

R.A. Evarestov

Department of Quantum Chemistry, St. Petersburg State University, Russia

R. Dittmann

Juelich Research Center, Germany

J. Maier

Max-Planck-Institute for Solid State Research, Stuttgart, Germany

Fe-doped SrTiO₃ became a model material for a wide class of mixed electronic-ionic conductors. Oxygen vacancies (V_O) and iron impurities in SrTiO₃, as well as their complexes, play a key role in electro-optical applications and non-volatile resistive random access switching memories. For example, the understanding of the relative spatial distribution of Fe ions and V_O is important to explain the formation of the conductive filaments. Recently Fe impurities (substituting B-type cations) and V_O in SrTiO₃ — separated and associated — have been addressed by a number of approaches. We performed detailed study of these defect complexes in a close collaboration with the two German partners: Juelich Research center and Max Planck Institute for Solid State research in Stuttgart.

The combined use of *ab initio* quantum mechanical and x-ray absorption near edge structure (XANES) methods confirms that the oxygen vacancies are located in the first coordination shell of Fe³⁺ ions in the cathod region of electro-colored Fe³⁺-doped SrTiO₃.

The binding energy of such a complex is estimated as ~ 0.4 eV. The lattice distortions obtained in *ab initio* modeling and extended x-ray absorption fine structure (EXAFS) experiments are in a very good agreement (Fig.13). The predicted distortions make a minor effect on a simulated XANES signal, and its shape mainly depends on the presence of V_O in the Fe^{3+} first coordination shell. Additionally, formation of the $Fe^{3+} V_O$ complex leads to disappearance of the phonon frequencies in the range $620\text{--}760\text{ cm}^{-1}$ of the calculated phonon spectrum which could be used for its identification.

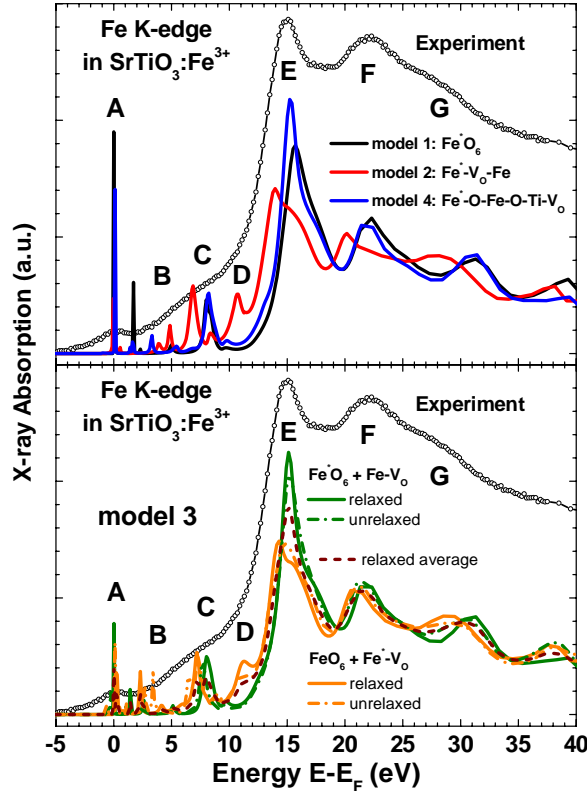


Figure 13. Comparison of the experimental and calculated Fe K-edge XANES spectra. For the model 3 the XANES spectra for the two relaxed (unrelaxed) Fe sites are shown by solid (dash-dotted) lines, and the average XANES spectrum for relaxed structure is shown by dashed line. The zero of energy scale corresponds to the theoretical Fermi level E_F .

MATERIALS FOR SOLID OXIDE FUEL CELLS: *ab initio* STUDY OF OXYGEN DEFECTS IN COMPLEX PEROVSKITES

Yu.A. Mastrikov, E.A. Kotomin,

R. Merkle, J. Maier

Max Planck Institute for Solid State Research, Stuttgart, Germany

M.M. Kukulja

Materials Science and Engineering Department, University of Maryland, USA

(La,Sr)(Co,Fe)O₃ (LSCF) -type perovskite solid solutions are used as mixed conducting SOFC cathode materials and oxygen permeation membranes. In a close collaboration with Max Planck Institute for Solid State Research in Germany and University of Maryland,

USA, the formation and migration of oxygen vacancies was studied in detail by means of first principles density functional calculations. Structure distortions, charge redistributions and transition state energies during the oxygen ion migration were obtained and analyzed. Both the overall chemical composition and vacancy formation energy are found to have only small impact on the migration barrier; it is rather the local cation configuration which affects the barrier. The electron charge transfer from the migrating O ion towards the transition metal ion in the transition state is much smaller in LSCF compared to BSCF perovskites where such a charge transfer makes a significant contribution to the low migration barriers observed (in particular for high Ba and Co content).

The oxygen migration occurs via the vacancy mechanism. The oxygen ion passage through the "critical triangle" formed by one B site cation and two A site cations (Fig 14) is the bottleneck; the trajectory is slightly curved away from the B site cation. In LSCF perovskites, the oxygen vacancy diffusion coefficients were experimentally found to be almost independent upon the cation composition, with a typical migration barrier of 0.8 eV. In contrast, BSCF perovskites exhibit a higher diffusivity with migration barriers as low as 0.5 eV, in particular, for samples with high Ba and Co content. In our calculations we explain how this is related to the peculiarities of the atomic and electronic structure of these two compounds.

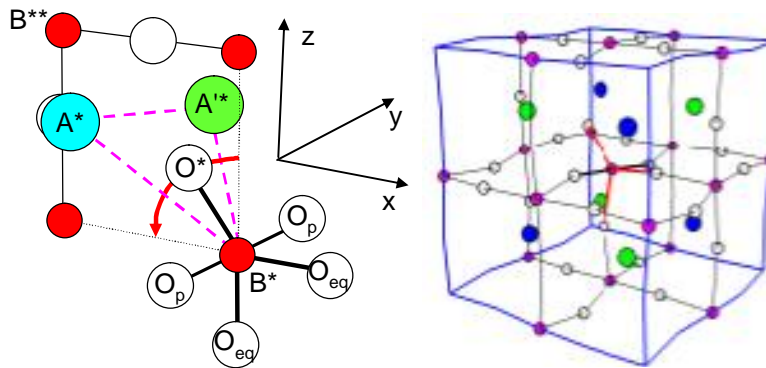


Figure 14. (left) Sketch of the oxygen ion migration path in ABO₃ perovskites through the "critical triangle" formed by one B-site cation B* and two A-site cations A*, A'. (right) The transition state structure distortion for the oxygen migration in LSCF.

Ab initio THERMODYNAMIC STUDY OF PEROVSKITE SOLID SOLUTIONS

Yu.A. Mastrikov, E.A. Kotomin,

D. Fuks

Ben Gurion University of the Negev, Beer Sheva, Israel

J. Maier

Max Planck Institute for Solid State Research, Germany

ABO₃-type perovskite solid solutions, e.g. Ba_xSr_{1-x}Co_{1-y}Fe_yO_{3-δ} (BSCF), are considered to be promising materials for applications as cathodes of solid oxide fuel cells (SOFC), oxygen permeation membranes and oxygen evolution catalysis. The small oxygen vacancy

formation energy characteristic for BSCF leads to high oxygen vacancy concentration, whilst a low oxygen vacancy migration barrier causes the high ionic mobility. These are two key factors leading to fast oxygen exchange of these materials and hence to their potential role in the context of energy conversion. However, a serious disadvantage of BSCF is its intrinsic instability at intermediate temperatures which leads to a slow transformation into a mixture of several phases, including a hexagonal phase with strongly reduced oxygen diffusivity as well as surface exchange rate.

The OSFC cathode performance could strongly depend on the morphology of these materials, remaining a single phase or two-phase mixture. Combining *ab initio* calculations of the atomic and electronic structure of different supercells with thermodynamics of solid solutions, we have constructed and discussed phase diagrams of several important BSCF chemical compositions. It was demonstrated (Fig. 15) that in BSC cobaltite solid solution the spinodal decomposition may occur already at relatively low temperatures, while ferrite (BSF and SCF) solid solutions decompose at relatively high temperatures forming a two-phase system where the coexisting hexagonal and cubic phases significantly differ in fractions of constituents.

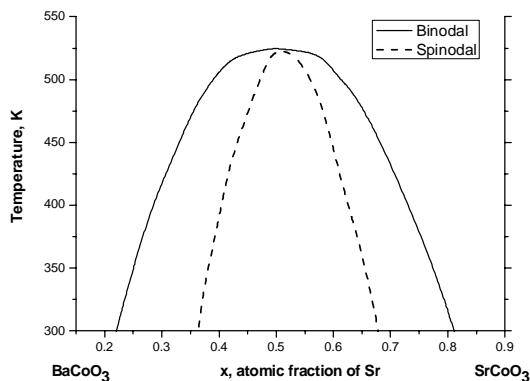


Figure 15. Quasi-binary phase diagram for $\text{Ba}_{1-x}\text{Sr}_x\text{CoO}_3$ solid solution. The solid line is the solubility (binodal) curve, dashed line shows the region of the spinodal decomposition.

AB INITIO CALCULATIONS OF THE ATOMIC AND ELECTRONIC STRUCTURE OF BaZrO_3 AND BaTiO_3 (111) SURFACES AND DEFECTS IN SrF_2

R.I. Eglitis

We performed the calculations of surface relaxations and energetics for the polar (111) surface of BaZrO_3 using a hybrid B3LYP description of exchange and correlation. On the (111) surface, both Zr- and BaO_3 -terminations were analyzed. For both Zr and BaO_3 -terminated BaZrO_3 (111) surfaces upper layer atoms, with the sole exception of BaO_3 -terminated surface Ba atom, relax inwards. The Zr-terminated BaZrO_3 (111) surface second layer Ba atom exhibits the strongest relaxation between all Zr and BaO_3 -terminated BaZrO_3 (111) surface atoms. The calculated surface relaxation energy for Zr-terminated BaZrO_3 (111) surface is almost fifteen times larger than the surface relaxation energy for BaO_3 -terminated BaZrO_3 (111) surface. The surface energy for Zr-terminated BaZrO_3 (111) surface (7.94 eV/cell) is smaller, than the surface energy for BaO_3 -terminated (111) surface

(9.33 eV/cell). The calculated BaZrO₃ optical bulk band gap, 4.79 eV is in an excellent agreement with the experimental value, 5.00 eV. The calculated optical band gap for the Zr- and BaO₃-terminated BaZrO₃ (111) surfaces becomes smaller with respect to the bulk optical band gap [1].

Using a hybrid B3LYP approach, the surface relaxation has been also calculated for the two possible Ti and BaO₃ terminations of BaTiO₃ (111) surface. For both Ti and BaO₃-terminations of (111) surface, the upper layer atoms relax inwards. The second layer atoms, with the sole exception of Ti-terminated BaTiO₃ (111) surface Ba atom, relax outwards. The calculated surface relaxation energy for Ti-terminated BaTiO₃ (111) surface is more than two times larger than the surface relaxation energy for BaO₃-terminated BaTiO₃ (111) surface. The surface energy for Ti-terminated BaTiO₃ (111) surface (7.28 eV/cell) is smaller, than the surface energy for BaO₃-terminated (111) surface (8.40 eV/cell)

AB INITIO SIMULATIONS OF POINT DEFECTS (VACANCIES) AND ATOM SUBSTITUTES (O AND Y) IN *fcc*-Fe LATTICE

A. Gopejenko, Yu.F. Zhukovskii, E.A. Kotomin

A. Möslang, P.V. Vladimirov

*Institut für Angewandte Materialien, Karlsruhe Institut für Technologie (KIT),
Karlsruhe, Germany*

V.A. Borodin

State Research Center "Kurchatov Institute", Moscow, Russia

To understand the mechanism of ODS particle formation in EUROFER steels, we simulated various equilibrium configurations of Y, O impurity atoms and Fe vacancies in steel matrix as well as their interactions and internal migration trajectories. *At the first stage* of this modeling, *ab initio* spin-frozen calculations using DFT-PW method with PW91 non-local Hamiltonian (as implemented in VASP code) have been performed on the lattice of high-temperature paramagnetic *fcc*-Fe phase.

Fig. 16 shows its 3×3×3 supercell with 2 Y substitute atoms located in the adjacent regular lattice sites and one O atom positioned in the nearest octahedral interstitial site. Our main interest was focused on: (i) interaction energies between the defects and (ii) defect migration energies as these data are then used as calculation parameters *at the second stage* of modeling when performing the lattice kinetic Monte-Carlo (LKMC) simulations of Y₂O₃ nanocluster growth in *fcc*-Fe crystal with various cluster configurations.

Our previous calculations showed an important role of the vacancies in the formation of the Y₂O₃ nanoclusters. To reduce both the defect concentration and interactions between periodic images of defects it has been necessary to increase the supercell size. Since 3×3×3 supercell did not provide yet satisfactory results of calculations on point defects, majority of previous calculations were performed for 4×4×4 *fcc*-Fe supercells. The last test calculations have been performed on perfect *fcc*-Fe lattice, to assess the minimum *k*-point mesh and cut-off energies required in order to achieve plausible results. To calculate the dependence of the results on the *k*-points mesh, the latter has been varied from 4×4×4 up to 9×9×9 and the cut-off energy has been fixed at 800 eV.

Our calculations clearly show that at least 7×7×7 *k*-point mesh is required to perform the calculations on the lattice composed from 5×5×5 supercells, application of which for

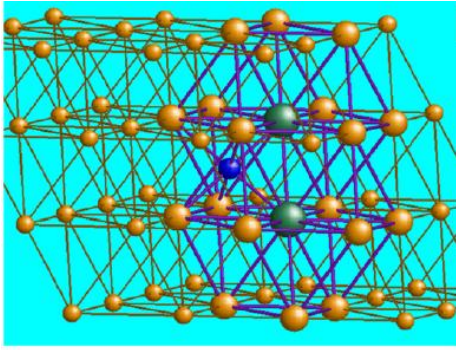


Figure 16. Supercell (SC) of γ -Fe crystal with two Y substitute and one O impurity atoms in the 1st nearest neighbor positions.

point defect calculations provides more realistic results as compared to those obtained for $4 \times 4 \times 4$ supercells as calculated previously. Due to dependence of a number of obtained results on the cut-off energy parameter as established in previous calculations, $7 \times 7 \times 7$ k -point mesh has been chosen and the cut-off energy has been varied from 700 to 800 eV.

As the results of $5 \times 5 \times 5$ SC calculations reproduced both qualitatively and semi-quantitatively the results received for $4 \times 4 \times 4$ SC, further variation of cut-off energy has not been required and the cut-off energy value of 800 eV has been used in further calculations since it was found to be optimal previously. It has been also necessary to perform the calculations of point defects in fcc -Fe lattice, in order to check if those results received in the calculations of $4 \times 4 \times 4$ supercell are reproducible within $5 \times 5 \times 5$ SC. In order to do this, the binding energies received within the calculations of $4 \times 4 \times 4$ and $5 \times 5 \times 5$ SCs between Y and vacancy have been compared. The corresponding results are present in Table 1 which clearly shows that the absolute values of E_{bind} between defects slightly decrease with SC increase which could be explained by the decreased influence of defect periodic images.

Table 1. Bonding in $Y_{Fe}-V_{Fe}$ pairs in γ -Fe

Supercell	$4 \times 4 \times 4$	$5 \times 5 \times 5$
Configuration	E_{bind} , eV*	E_{bind} , eV*
1-NN	1.67	1.42
2-NN	-0.21	-0.07
3-NN	0.30	0.14
4-NN	0.40	0.30

*binding energies

AB INITIO SIMULATIONS OF POINT DEFECTS (VACANCIES) AND ATOM SUBSTITUTES (O AND Y) IN bcc -Fe LATTICE

Yu.A. Mastrikov, Yu.F. Zhukovskii, E. Kotomin

A. Möslang, P.V. Vladimirov
*Institut für Angewandte Materialien, Karlsruhe Institut für Technologie,
 Karlsruhe, Germany*

Due to essential mismatch between the structures of Y_2O_3 (bixbyite phase) and α -Fe, yttrium solute atoms have to be stabilized in the iron matrix by vacancies. Then vacancies

could be healed by oxygen atoms, creating the bixbyite type of Y-O bonds. Since *bcc*-phase of iron is stable in a wide interval of temperatures and displays ferromagnetic properties, *ab initio* supercell calculations on pure and defective α -Fe have been performed in spin-polarized regime using the same DFT-PW approach as for γ -Fe and applying the non-local PBE exchange-correlation functional. The first stage of *ab initio* simulations on α -Fe has included possibilities of vacancy cluster creation in the corresponding lattice which stabilizes implementation of impurity atoms in the iron bulk. Atomic radius of Y atom is larger than that of Fe atom (0.18 and 0.14 nm respectively), which creates a strong repulsion between them inside an iron matrix.

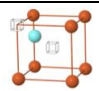
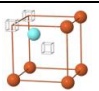
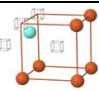
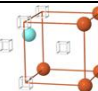
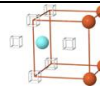
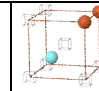
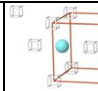
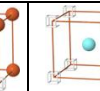
On the other hand, impurity Y atom can stably exist in iron lattice as a substitute only (Y_{Fe}). The repulsion between the two Y_{Fe} atoms could be reduced by creation of Fe vacancies. In *bcc* iron lattice, V_{Fe} vacancies can segregate, forming stable clusters (Tables 2, 3). Stabilization of Y impurity atom inside iron lattice could require more than one vacancy *per* solute atom. In such a case, not only substitute Y_{Fe} atom is stable but also yttrium atom located in interstitial sites (Y_i).

Table 2. Binding energies of multiple vacancies (V_{Fe})_N inside α -Fe lattice (as shown in Table 3).

N	1	2	3	4	5	6	7	8	9
$E_{bind}(N)$, eV	0.	0.23	0.65	1.38	2.19	3.18	2.94	4.23	5.34

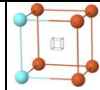
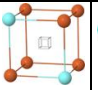
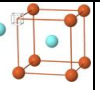
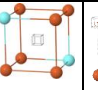
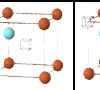
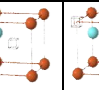
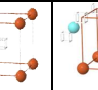
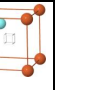
Size of vacancy cluster in the *bcc*-Fe lattice has been varied from one to nine vacancies in the $4 \times 4 \times 4$ supercell (Table 3). It has been shown that a growth of vacancy cluster is energetically favorable (Table 2). However, adding one more vacancy to the cluster of six vacancies requires, at least, 0.24 eV. So, clusters of six vacancies could be quite common defects in α -Fe matrix. Analogous calculations have been repeated for a single Y solute atom incorporated in different vacancy clusters (Table 3). As the reference energies, there are used isolated vacancies and isolated Y_{Fe} . In all the configurations, Y atom is positioned in the middle of vacancy cluster and all the corresponding defect complexes have been found energetically stable. As in the case of pure vacancy clusters (Table 2), incorporation of additional vacancy to the cluster containing Y_i atom and six vacancies in octahedral coordination around it (Table 3) is energetically unfavourable. Although the complex of Y_{Fe} atom and eight vacancies in cubic coordination around it has been found to be stable too, the binding energy for this configuration is smaller, than that for clusters containing six and eight vacancies with interstitial Y_i .

Table 3. Binding energy of single solute Y atom in vacancy clusters inside α -Fe lattice.

models								
N	2	3	4	5	6	7	8	8
$E_{bind}(N)$, eV	1.355	2.887	4.893	6.021	7.386	5.579	7.956	7.123

Calculations performed in order to estimate pair-wise Y-Y interaction in different positions of a single vacancy show a weak attraction of ~ 0.1 eV for impurity atoms at 2NN and 3NN distances (Table 4). For 5NN Y-Y distance along the direction [111], the interaction of -0.13 eV is repulsive. Other interactions at close inter-defect distances are

Table 4. Interactions of Y_{Fe} - Y_{Fe} pair with V_{Fe} (NN=1-3), Eq. as well as a single solute Y atom with either a pair of vacancies (NN=4-6), or the V_{Fe} - Y_i - V_{Fe} complex (NN=2) inside α -Fe lattice.

models								
NN distance	1	2	3	3	4	5	6	2
E_{bind} , eV	0.30	1.03	0.27	1.16	0.01	-0.13	-0.04	1.3

negligible small. Interaction of a single solute atom Y_{Fe} with the V_{Fe} - Y_i - V_{Fe} complex at different distances has been calculated (Table 4). At the distances of the 3NN and smaller, Y_{Fe} transforms V_{Fe} - Y_i - V_{Fe} complex into Y_{Fe} - V_{Fe} - Y_{Fe} configuration. The strongest attraction has been observed for the defect aligned along the [111] direction. Starting from the 4NN the interaction becomes weaker and does not exceed 0.15 eV. Interaction between the two V - Y_i - V complexes is attractive too. At three closest distances, without overlapping vacancies, binding energy between the complexes is about 1.3-1.4 eV. Thus, V_{Fe} can segregate, creating stable clusters, while Y impurity atoms can be stabilized by vacancies.

B. Kinetics of processes with self-organization

THEORY OF NON-EQUILIBRIUM CRITICAL PHENOMENA IN THREE-DIMENSIONAL CONDENSED SYSTEMS OF CHARGED MOBILE NANOPARTICLES

V.N. Kuzovkov, G. Zvejnieks, E.A. Kotomin

A study of 3d electrostatic self-assembly (SA) in systems of charged nanoparticles (NP) is one of the most difficult theoretical problems. In particular, the limiting case of negligible or very low polar media (*e.g.*, salt) concentration, where the long-range NPs interactions cannot be reduced to commonly used effective short-range (Yukawa) potentials, remains unstudied. Moreover, the present study has demonstrated that unlike the Debye-Hückel theory, a complete screening of the charges in SA kinetics is not always possible. Generally speaking, one has to take into account implicitly how each NP interacts

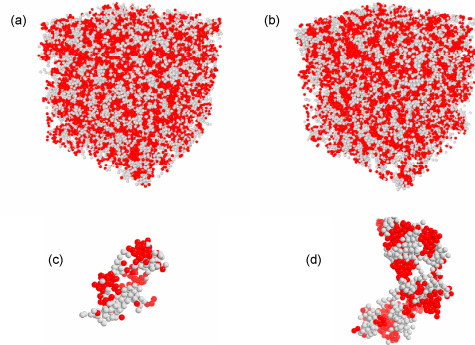


Figure 17. Characteristic 3d structure snapshots obtained using the RMC: (a,b) corresponds to two different times, whereas (c,d) show the maximal domain for snapshots (a,b).

with all other NPs (the true long-range interactions). Traditional theoretical methods allow us to monitor such the electrostatic 3d system kinetics only at very short times, which is far from sufficient for the understanding the dynamic SA. Combining an integrated analytical approach (nonlinear integro-differential kinetic equation for correlation functions) and reverse Monte Carlo in 3d case, we have obtained the self-consistent solution of this challenging problem (Fig. 17). We demonstrate, in particular, the existence of critical points and critical phenomena in the non-equilibrium kinetics in a 3d system of oppositely charged mobile NPs.

KINETIC MONTE CARLO MODELING OF REACTION-INDUCED PHASE SEPARATION IN Au/Ni(111) SURFACE ALLOY

G. Zvejnieks

A. Ibenskas, E.E. Tornau

Center for Physical Sciences and Technology, Semiconductor Physics Institute, Vilnius, Lithuania

Kinetic Monte Carlo (KMC) simulations of Au–Ni phase separation in Au/Ni(111) surface alloy during nickel carbonyl formation reaction were performed at room temperature by taking into account realistic rates of Au and Ni adatom diffusion and CO adsorption and desorption, while keeping the rate of nickel carbonyl formation reaction as a free parameter. We also obtained pair and three-body interaction constants between Au and Ni adatoms using the ab initio calculations and demonstrated that their proper choice is crucial for understanding the Au–Ni separation process.

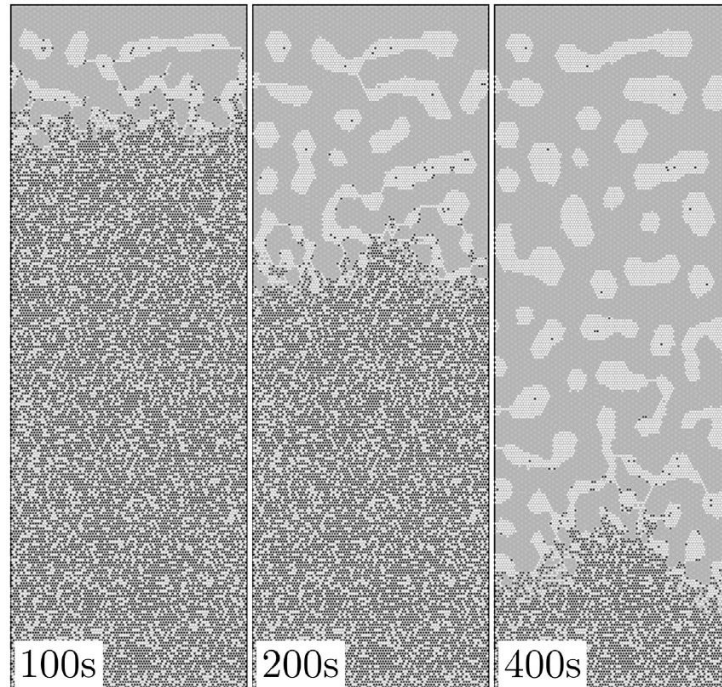


Figure 18. Snapshots of the Au/Ni(111) surface alloy instability kinetics computer simulation. Black, white and gray dots mark top monolayer Ni, Au adatoms and CO molecules, respectively. The reaction front moves from top to bottom.

Three regimes with qualitatively different Ni–CO reaction propagation kinetics in Au/Ni(111) surface alloy were found by varying the constants of trio-triangle interactions within the limits of their accuracy. The sensitivity of the proposed model to interaction parameters leads to the regimes that differ by step flow rate, Au islands formation mechanism(channel-type or homogenous flow), Au island contamination level by Ni impurities and reaction damping tendency at the reaction front. Nucleation of nickel-free Au islands was observed for a homogeneous step flow pattern, and the corresponding step flow rate is in a good quantitative agreement with existing experimental data.

ON PROPERTIES OF ELECTRON-HOLE PAIRS IN DIELECTRICS

E. Klotins

The electron-hole pair is a central concept addressed to problems of advanced materials and, generally, comprising both the fundamental questions and applications in optics. A guiding principle in the theoretical description is to identify a system as an effective vacuum with the electrons and holes as elementary excitations of that vacuum. In these terms the first goal is how to describe the ground state of the system and, then, the excited states playing a central role in determining the measurable quantities of the light-matter interaction.

Two basic approaches are considered with emphasis on their conceptual background and mathematical techniques. The first is the semiconductor-light Hamiltonian (SC) approach, where the system with well separated bands is excited by a classic electromagnetic field in the RWA approximation. This allows a connection of the creation-annihilation operators for electrons and holes with the exciton operators as the single entities constituting in this way an effective single-particle theory for electron-hole pairs, excitons and their interactions. Restrictions of the SC approach appear in strong field nonlinear and non-adiabatic effects that are fundamental and cannot be abandoned within the existing RWA and the subsequent perturbation approaches. Within the conceptual level the SC approach is based on the Schrödinger's equation with is not Lorentz covariant, and therefore excludes applications where the relativistic effects are essential.

In contrast, the quantum electrodynamics formalism for electron-hole pairs represents a soluble case, i.e. a model resembling the Diracs picture for a two-band dielectric. The excitation of electron-hole pairs is quantified as a Klein-Gordon field, with input entities supported by SC type calculations, namely, dispersion relations for the electron and hole, the band gap between valence and conduction bands as well as symmetry properties of the Brillouin zone.

The rationale find from these prototypic approaches is a kinetic theory based on dynamical foundation. It allows to calculate non-equilibrium distribution function and the relevant physical quantities far from equilibrium. A problem non resolved yet is generalization of this Klein-Gordon formalism to more complicated fermion-fermion interactions and inclusion of electron-phonon interaction as highly motivated subjects in the future work.

C. Plasma Physics

RMP ELM SUPPRESSION ANALYSIS BY MEANS OF LOW-DIMENSIONAL MODEL SYSTEM FOR QUASI-PERIODIC PLASMA PERTURBATIONS

O. Dumbrajs,

D. Constantinescu

University of Craiova, Association Euratom-MECI, Romania

V. Igochine, K. Lackner, H. Zohm and ASDEX Upgrade team

Max-Planck Institut für Plasmaphysik, Association Euratom-IPP, Germany

Edge localized modes (ELM) are a significant concern in magnetically confined toroidal fusion plasmas because they can rapidly erode plasma facing material surfaces, cause edge melting and surface cracking. They also reduce the coupling efficiency of rf antennas and trigger other MHD instabilities. The importance of ELM control was realized many years ago and different means of their control were developed. ELM suppression/control is required for a steady state operation of the International Thermonuclear Experimental Reactor (ITER). The natural ELM frequency should be decreased by a factor ~ 30 . Two main control strategies are foreseen for ITER: 1) injection of small deuterium pellets, 2) resonant magnetic perturbations (RMP). We investigate possible mechanisms of RMP ELM suppression in a low-dimensional model system for quasi-periodic plasma perturbations.

EFFECT OF ELECTRON BEAM MISALIGNMENTS ON GIROTRON EFFICIENCY

O. Dumbrajs,

G. S. Nusinovich

University of Maryland, College Park, MD, USA

The theory describing the operation of gyrotrons with tilted and shifted electron beams has been developed. Effects of the tilt and shift are studied for a 1 MW, 170 GHz gyrotron,

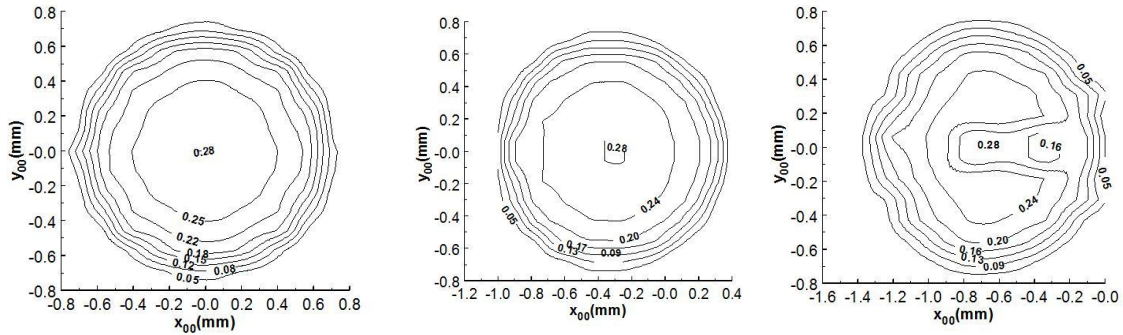


Figure 19. Efficiency as a function of transverse coordinates in the cases of (a) parallel displacement, (b) a tilt angle 0.5° and (c) a tilt angle 1° .

which is presently under development in Europe for electron cyclotron resonance plasma heating and current drive in the ITER. It is shown that one should expect significant deterioration of gyrotron operation in such gyrotrons when the tilt angle exceeds $0.4\text{-}0.5^\circ$ and the parallel shift of the beam axis with respect to the axis of a microwave circuit is larger than $0.4\text{-}0.5$ mm. At the same time, simultaneous tilting and shifting in a proper manner can mitigate this deteriorating effect.

D. EXPERIMENTAL STUDIES

COMPARATIVE STUDY OF LUMINESCENCE PROPERTIES OF MACRO- AND NANOCRYSTALLINE MgO USING SYNCHROTRON RADIATION

A.I. Popov, L. Shirmane, V. Pankratov, G. Chikvaidze

A. Lushchik,

Institute of Physics, University of Tartu, Estonia

A. Kotlov

HASYLAB, DESY, Notkestrasse 85, Hamburg D-22761, Germany

V.E. Serga, L.D. Kulikova

Institute of Inorganic Chemistry, Riga Technical University, Latvia

J. Zimmermann

Institute of Materials Science, Darmstadt University of Technology, Germany

Wide band-gap MgO ($E_g = 7.8$ eV) continues to attract great attention due to its fundamental interest and applications. The goal of the present study was to compare the luminescent properties of nanocrystalline MgO which was prepared by the extractive-pyrolytic method with macrocrystalline powder analogues and a single crystal. Special attention was paid to VUV spectral range, which is not reachable with commonly lamp and laser sources used. The SUPERLUMI facility of HASYLAB at DESY was used for the measurements of emission and excitation spectra.

Fig. 20 shows the excitation luminescence spectra for all these three samples measured at 2.95 eV (420 nm) in spectral range 4.5–10.0 eV. Two definite conclusions can be drawn here, namely: (a) In both macropowder and single crystal sample, the well-known 5.7 eV excitation band caused by deformation-induced defects/vacancy complexes is revealed. The appropriate peak for nanoparticle samples reveals blue shift at about 0.3 eV, which could be connected with the nano-size of particles. (b) The excitation spectra for both macro- and nano-particle samples show the clear shoulder at about 5.0 eV, where the both F and F^+ centers have their optical absorption with peak essentially at the same energy of ~ 5.0 eV, while such feature is absent at all in the case of single crystals. (c) in the case of MgO single crystal, the exciton peak is quite well resolved, while in the case of macro and nano powder materials, its exact position is not easy to determine.

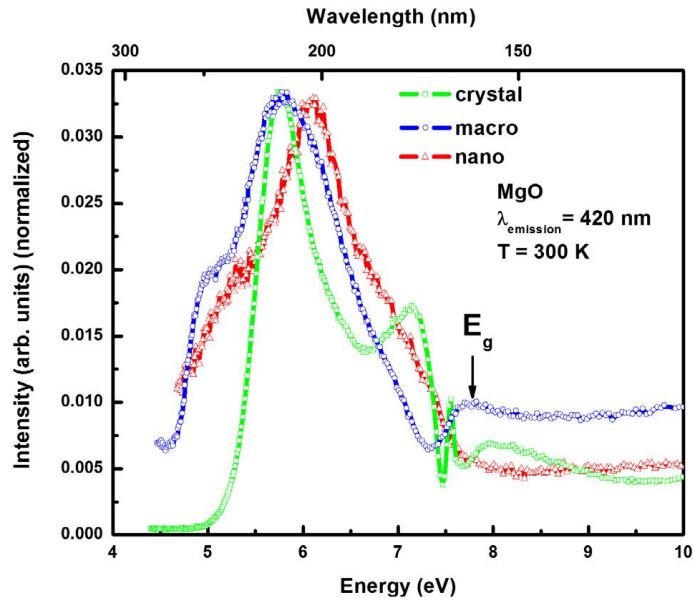


Figure 20. MgO excitation spectra for nano- and macro-samples.

BiI₃ NANOCCLUSERS IN MELT-GROWN CdI₂ CRYSTALS STUDIED BY OPTICAL ABSORPTION SPECTROSCOPY

A.I. Popov, V. Pankratov

I.Karbovnyk, V. Lesivtsiv, I. Bolesta, S. Velgosh I. Rovetsky
Ivan Franko National University of Lviv, Ukraine

C. Balasubramanian

Institute for Plasma Research, Bhat, Gandhinagar 382 044, India

Cadmium iodide (CdI₂) is a well known layered-structure compound. Both pure and doped CdI₂ crystals have demonstrated several potentially attractive applications as scintillator and photochromic materials, candidate materials for memory elements, electroplating and lithography.

We studied optical absorption of CdI₂ crystals doped by BiI₃ (1 mol %) in the temperature range of 77–300 K. Complex structure of the optical absorption spectra of these crystals was discussed with the particular focus on clusters contribution to the optical properties of the investigated material.

The main absorption, observed in these crystals at 2.59 eV is related to quantum confined exciton absorption of bimolecular BiI₃ cluster. BiI₃ centers that are formed by substitution of three Cd²⁺ ions for two Bi³⁺ ions. Considering the spectral shift of this peak in CdI₂–BiI₃ with respect to the bulk BiI₃, the radius of the bimolecular cluster of BiI₃ ($R \approx 14$ Å) has been roughly estimated. Bands peaked at higher energies (found in thin samples) are attributed to higher energy states of an exciton confined within the BiI₃ cluster. The possible origin of long-wavelength absorption peaks could be attributed to larger clusters, as shown in the following Table:

Peak position, eV	Width (eV)	Origin
1.94	0.11	6- (or more) molecules BiI ₃ clusters
2.06	0.19	4-molecules BiI ₃ clusters and
2.38	0.38	4-molecules BiI ₃ clusters
2.59	0.44	Bimolecular BiI ₃ clusters
2.84	0.18	?
3.03	0.20	?
3.27	0.22	?

LUMINESCENCE AND ULTRAVIOLET EXCITATION SPECTROSCOPY SrI₂ AND SrI₂:Eu²⁺

V. Pankratov, A.I. Popov, L. Shirmane

A. Kotlov

HASYLAB at DESY, Notkestrasse 85, D-22607 Hamburg, Germany

G.A. Bizarri

Lawrence Berkeley National Laboratory, Berkeley, CA 94720, USA

A. Burger, P. Bhattacharya, E. Tupitsyn, E. Rowe, V.M. Buliga

Fisk University, Nashville, USA

R.T. Williams

Department of Physics, Wake Forest University, Winston-Salem, North Carolina, USA

In the renewed search for high resolution γ -ray scintillators within the last decade, improved SrI₂ crystals grown by the Bridgeman technique were found to have exceptional light yield of about 90,000 photons/MeV.

We report measurements of luminescence and its ultraviolet excitation spectra in SrI₂ and SrI₂:Eu²⁺ at temperatures of 10 and 300 K. Excitation spectroscopy technique using synchrotron radiation (SUPERLUMI facility of HASYLAB at DESY) was applied.

Excitonic properties in nominally pure and europium doped crystals have been studied. Special attention is focused on determining the exciton energy (5.12 eV \pm 0.1 eV at RT) and its temperature shift (namely, thermal peak shift of the 1s exciton in SrI₂ from 10 K to 300 to be about 0.35 eV) from features of the excitation spectra, on observation of a broadened Eu emission band attributed to trace Eu associated with oxygen in nominally undoped crystals, and on adding observations concerning the 3.4 eV band at low temperature attributed to the self-trapped exciton.

Defence of Master Science Thesis

MSc Thesis-- A. Sorokin „First principles thermodynamic calculations on Al-doped ZnO“ was successfully defended in the end of May, 2013, at the University of Latvia.

Publications in 2013 Year

SCI

1. D. Fuks, **Yu. Mastrikov**, **E.A. Kotomin**, and J. Maier, *Ab initio* thermodynamic study of (Ba,Sr)(Co,Fe)O₃ perovskite solid solutions for fuel cell applications. - J. Mater. Chem. A, 2013, **1**, p. 14320–14328.
2. **Yu.F. Zhukovskii**, **S. Piskunov**, **J. Kazerovskis**, D.V. Makaev, and P.N. D'yachkov, Comparative theoretical analysis of BN nanotubes doped with Al, P, Ga, As, In, and Sb.- J. Phys. Chem. C, 2013, **117**, p. 14235–14240.
3. **D. Gryaznov**, E. Blokhin, **A. Sorokin**, **E.A. Kotomin**, R.A. Evarestov, A. Bussmann-Holder, and J. Maier, A comparative *ab initio* thermodynamic study of oxygen vacancies in ZnO and SrTiO₃: emphasis on phonon contribution. - J. Phys. Chem. C, 2013, **117**, p. 13776–13784.
4. M.M. Kuklja, **E.A. Kotomin**, R. Merkle, **Yu.A. Mastrikov**, and J. Maier, Combined theoretical and experimental analysis of processes determining cathode performance in solid oxide fuel cells. - Phys. Chem. Chem. Phys., 2013, **15**, p. 5443-5471.
5. **Yu.A. Mastrikov**, R. Merkle, **E.A. Kotomin**, M.M. Kuklja, and J. Maier, Formation and migration of oxygen vacancies in La_{1-x}Sr_xCo_{1-y}Fe_yO_{3-δ} perovskites: insight from *ab initio* calculations and comparison with Ba_{1-x}Sr_xCo_{1-y}Fe_yO_{3-δ}. - Phys. Chem. Chem. Phys., 2013, **15**, p. 911 - 918.
6. E. Blokhin, **E.A. Kotomin**, A. Kuzmin, J. Purans, R.A. Evarestov, and J. Maier, Theoretical modeling of the complexes of iron impurities and oxygen vacancies in SrTiO₃. - Appl. Phys. Lett., 2013, **102**, 112913 (p. 1-5).
7. **J. Kazerovskis**, **S. Piskunov**, **Yu.F. Zhukovskii**, P.N. D'yachkov, and S. Bellucci, Formation of linear Ni nanochains inside carbon nanotubes: Prediction from density functional theory. - Chem. Phys. Lett., 2013, **577**, p. 92-95.
8. A. Weizman, D. Fuks, **E.A. Kotomin**, and **D. Gryaznov**, *Ab initio* study of phase competition in (La_{1-c},Sr_c)CoO₃ solid solutions. - Solid State Ionics, 2013, **230**, p. 32–36.
9. M.M. Kuklja, **Yu.A. Mastrikov**, B. Jansang, and **E.A. Kotomin**, First principles calculations of (Ba,Sr)(Co,Fe)O_{3-δ} structural stability. - Solid State Ionics, 2013, **230**, p. 21–26.
10. **R.I. Eglitis**, *Ab initio* calculations of the atomic and electronic structure of BaZrO₃(111) surfaces. - Solid State Ionics, 2013, **230**, p. 43-47.
11. H. Shi, L. Chang, R. Jia, and **R.I. Eglitis**, *Ab initio* calculations for the *F*-center transfer and *R* centers in SrF₂. - Comput. Mater. Sci., 2013, **79**, p. 527-533.
12. R. Jia, Z. Yi, C. Liu, H. Shi, H. Zhang, and **R.I. Eglitis**, First principles studies of the self trapped hole and the fluorine adsorption on the SrF₂ (111) surface. - Comput. Mater. Sci., 2013, **73**, p. 9-14.

13. R.A. Evarestov and **Yu.F. Zhukovskii**, Four-faceted nanowires generated from densely-packed TiO₂ rutile surfaces: *Ab initio* calculations. - Surf. Sci., 2013, **608**, p. 226–240.
14. **Yu.F. Zhukovskii**, **S. Piskunov**, **J. Begens**, **J. Kazerovskis**, and **O. Lisovski**, First-principles calculations of point defects in inorganic nanotubes. - Phys. Status Solidi B, 2013, **250**, p. 793-800.
15. D. Fuks, A. Weizman, and **E.A. Kotomin**, Phase competition in (La,Sr) CoO₃ solid solutions: *ab initio* thermodynamic study. - Phys. Status Solidi B, 2013, **250**, p. 864-869.
16. I. Karbovnyk, V. Lesivtsiv, I. Bolesta, S. Velgosh, I. Rovetsky, V. Pankratov, C. Balasubramanian, and **A.I. Popov**, BiI₃ nanoclusters in melt-grown CdI₂ crystals studied by optical absorption spectroscopy. - Physica B, 2013, **413**, p. 12–14.
17. **A.I. Popov**, L. Shirmane, V. Pankratov, A. Lushchik, A. Kotlov, V.E. Serga, L.D. Kulikova, G. Chikvaidze, and J. Zimmermann, Comparative study of the luminescence properties of macro- and nanocrystalline MgO using synchrotron radiation. - Nucl. Instr. Meth. B, 2013, **310**, p. 23-26.
18. **D. Bocharov**, **D. Gryaznov**, **Yu.F. Zhukovskii**, and **E.A. Kotomin**, *Ab initio* simulations of oxygen interaction with surfaces and interfaces in uranium mononitride. - J. Nucl. Mater., 2013, **435**, p. 102–106.
19. **R.I. Eglitis**, *Ab initio* calculations of BaTiO₃(111) surfaces. - Phase Transitions, 2013, **86**, p. 1115 - 1120.
20. V. Pankratov, **A.I. Popov**, L. Shirmane, A. Kotlov, G.A. Bizarri, A. Burger, P. Bhattacharya, E. Tupitsyn, E. Rowe, V.M. Buliga, and R.T. Williams, Luminescence and ultraviolet excitation spectroscopy of SrI₂ and SrI₂:Eu²⁺. - Radiat. Meas., 2013, **56**, p. 13-17.
21. **E. Klotins** and **G. Zvejnieks**, Quantum chemical study of electron-phonon interaction in crystals. - Phys. Status Solidi C, 2013, **10**, p. 705–708.
22. A. Dauletbekova, F. Abuova, A. Akilbekov, **E.A. Kotomin**, and **S. Piskunov**, First-principles modeling of the *H* color centers in MgF₂ crystals. - Phys. Status Solidi C, 2013, **10**, p. 160–164.
23. A. Usseinov, **E.A. Kotomin**, **Yu.F. Zhukovskii**, J. Purans, **A. Sorokin**, and A.T. Akilbekov, Atomic and electronic structure of hydrogen on ZnO (10-10) surface: *ab initio* hybrid calculations. - IOP Conf. Series: Mater. Sci. Engineering, 2013, **49**, 012054 (p. 1-4).
24. E. Blokhin, R.A. Evarestov, **D. Gryaznov**, **E.A. Kotomin**, and J. Maier, Theoretical modeling of antiferrodistortive phase transition for SrTiO₃ ultrathin films. - Phys. Rev. B, 2013, **88**, 241407 (p. 1-4).
25. **O. Dumbrajs** and G.S. Nusinovich Effect of electron beam misalignments on the gyrotron efficiency.-- Phys. Plasmas **20**, 073105 (2013).

Non-SCI papers

1. O. Dumbrajs, Žirotrons - megavatu mikroviļņu avots kodolplazmas uzkaršēšanai. - *Enerģija un pasaule*, 2013, 2, p. 74-78.
2. S. Piskunov, J. Kazerovskis, Yu.F. Zhukovskii, P.N. Dyachkov, and S. Bellucci, Incorporation of Ni nanofilament inside carbon nanotubes: DFT calculations. - Proc. Intern. Conf. „Physics, Chemistry and Application of Nanostructures (Nanomeeting-2013, Minsk, Belarus)” (Eds. V.E. Borisenko, S.V. Gaponenko, V.S. Gurin, and C.H. Kam; World Scientific, New Jersey, London, Singapore), 2013, p. 139-142.
3. Yu.N. Shunin, V.I. Gopeyenko, N. Burlutskaya, T. Lobanova-Shunina, and S. Bellucci, Electromagnetic properties of CNTs and GNRs based nanostructures for nanosensor systems. - Proc. Intern. Conf. „Physics, Chemistry and Application of Nanostructures (Nanomeeting-2013, Minsk, Belarus)” (Eds. V.E. Borisenko, S.V. Gaponenko, V.S. Gurin, and C.H. Kam; World Scientific, New Jersey, London, Singapore), 2013, p. 250-253.
4. Yu.F. Zhukovskii, S. Piskunov, O. Lisovski, and J. Begens, First principles simulations on doped TiO₂ and SrTiO₃ nanotubular photocatalysts for water-splitting hydrogen generation. - Proc. Intern. Conf. „Physics, Chemistry and Application of Nanostructures (Nanomeeting-2013, Minsk, Belarus)” (Eds. V.E. Borisenko, S.V. Gaponenko, V.S. Gurin, and C.H. Kam; World Scientific, New Jersey, London, Singapore), 2013, p. 513-516

Chapters in Scientific Books

E.A. Kotomin, R. Merkle, **Yu.A. Mastrikov**, M.M. Kuklja, and J. Maier, Energy Conversion: Solid Oxide Fuel Cells. First-Principles Modeling of Elementary Processes. - Chapter 6 in book: *Computational Approaches to Energy Materials* (eds. A.Walsch, A. Sokol, C.R.A. Catlow, Wiley), 2013, p. 149-186.

Presentations at Scientific Conferences, Congresses, Meetings, Schools and Workshops

I. 29th ISSP Conference (Riga, Latvia, February, 2013).

1. D. Constantinescu, O. Dumbrajs, V. Igochine, K. Lackner, H. Zohm, and ASDEX Upgrade team, "Edge localized mode suppression by means of resonant magnetic perturbations". Abstracts: p. 23.
2. J. Begens, S. Piskunov, and Yu.F. Zhukovskii, "Quantum chemical simulations of doped SrTiO₃ nanotubes for application in photocatalytic reactions". Abstracts: p. 25.
3. A. Anspoks, D. Bocharov, J. Purans, F. Rocca, and V.A. Trepakov, "Local structure analysis of SrTiO₃ and SrTi¹⁸O₃ by X-ray absorption spectroscopy". Abstracts: p. 34.
4. A. Sorokin, Yu.F. Zhukovskii, D. Gryaznov, J. Purans, and E.A. Kotomin, "Temperature dependence of thermodynamic properties of oxygen vacancies in ZnO: first-principle calculations". Abstracts: p. 35.
5. J. Kazerovskis, S. Piskunov, and Yu.F. Zhukovskii, "Atomic and electronic properties of Ni nanofilament encapsulated inside single-walled nanotubes of different chiralities". Abstracts: p. 36.
6. R.I. Eglitis, H. Shi, R. Jia, and L. Chang, "First-principles calculations of hydroxyl impurities in CaF₂ and BaF₂ crystals". Abstracts: p. 55.
7. A. Gopejenko, Yu.F. Zhukovskii, P.V. Vladimirov, E.A. Kotomin, Yu.A. Mastrikov, and A. Möslang, "Ab initio calculations of Y and vacancies interactions in fcc Fe lattice". Abstracts: p. 61.
8. A. Anspoks, D. Bocharov, J. Purans, F. Rocca, A. Sharakovskis, and V.A. Trepakov, "X-ray absorption spectroscopy and second harmonic generation analysis of SrTi¹⁸O₃". Abstracts: p. 85.
9. Yu.N. Shunin, Yu.F. Zhukovskii, V. Gopeyenko, T. Lobanova-Shunina, N. Burlutskaya, and S. Bellucci, "GNRs and CNTs based nanosensor systems modelling". Abstracts: p. 103.

II. 47th Russian School on Condensed State Physics (St. Petersburg, Russia, March, 2013).

10. P. Zhgun, D. Bocharov, S. Piskunov, A. Kuzmin, and J. Purans, "Quantum chemistry calculations on ScF₃ electronic structure and lattice dynamics". Abstracts: p. 65.

III. 10th Symposium on Fuel Cell as well as Battery Modelling and Experimental Validation (ModVal-10) (Bad Boll, Germany, March, 2013).

11. R. Merkle, L. Wang, Yu.A. Mastrikov, E.A. Kotomin, M.M. Kuklja, and J. Maier, "Oxygen exchange mechanism on mixed conducting perovskites: insight from experiment and theory." - Abstracts: p. 37.

IV. 11th International Conference "Information Technologies and Management", IT&M'2013 (Riga, Latvia, April, 2013).

12. Yu.N. Shunin, Yu.F. Zhukovskii, V.I Gopeyenko, T. Lobanova-Shunina, N. Burlutskaya, and S. Bellucci, "Carbon-based nanosensor systems: modelling and technology". Abstracts: p. 17-18.
13. J. Kazerovskis, S. Piskunov, and Yu.F. Zhukovskii, "First principles simulations on Ni nanofilaments incorporated in carbon nanotubes". Abstracts: p. 53.

14. **Yu.F. Zhukovskii, S. Piskunov, O. Lisovski, and J. Begens**, "Doped TiO₂ and SrTiO₃ nanotubular photocatalysts for water-splitting hydrogen generation: First principles simulations". Abstracts: p. 80-82.

15. **S. Piskunov and Yu.F. Zhukovskii**, "BN nanotubes doped by Al, P, Ga, As, In, and Sb: Predictions from first principles". Abstracts: p. 110-111.

16. **A. Gopejenko, Yu.F. Zhukovskii, P.V. Vladimirov, E.A. Kotomin, Yu.A. Mastrikov, and A. Möslang**, "First principles modeling of interactions between Y, O and vacancies in fcc-Fe lattice". Abstracts: p. 112-114.

V. 9th International Conference "Functional Materials and Nanotechnologies" FM&NT-2013 (Tartu, Estonia, April, 2013).

17. **A.I. Popov and G.J. McIntyre**, "Photostimulable storage phosphors and image-plate development for neutron imaging". – Abstract: OR-11.

18. **A. Anspoks, D. Bocharov, J. Purans, F. Rocca, A. Sarakovskis, V.A. Trepakov, A. Dejneka, and M. Itoh**, "Local structure studies of SrTi¹⁶O₃ and SrTi¹⁸O₃". – Abstract: OR-15.

19. **Yu.N. Shunin, Yu.F. Zhukovskii, V.I. Gopeyenko, N. Burlutskaya, T. Lobanova-Shunina, and S. Bellucci**, "Electromagnetic properties of interconnects in nanodevices based on CNT, GNR and graphene aerogels." – Abstract: OR-28.

20. **G. Zvejnieks, P. Merzlyakov, V.N. Kuzovkov, and E.A. Kotomin**, "Cellular automata modeling of void lattice self-organization in CaF₂ under irradiation." – Abstract: OR-29.

21. **Yu.F. Zhukovskii, A. Gopejenko, Yu.A. Mastrikov, E.A. Kotomin, P.V. Vladimirov, and A. Möslang**, "Modeling of Y-O precipitation in bcc-Fe and fcc-Fe lattices." – Abstract: OR-35.

22. **E.A. Kotomin, M.M. Kuklja, Yu.A. Mastrikov, O. Sharia, D. Fuks, and J. Maier**, "Prediction of structural stability of complex perovskites for solid oxide fuel cells from first principles." – Abstract: OR-36.

23. **E. Klotins and G. Zvejnieks**, "Electron-phonon interactions: spatial localization." – Abstract: OR-44.

24. **P. Merzlyakov, G. Zvejnieks, V.N. Kuzovkov, and E.A. Kotomin**, "Statistical analysis of void lattice formation in CaF₂." – Abstract: PO-30.

25. **A.I. Popov, V. Savchyn, J. Purans, A. Dabrowska, A. Huczko, B. Pathak, and D.P. Subedi**, "Cathodoluminescence study of Al-doped ZnO nanofilms." – Abstract: PO-78.

26. **F.U. Abuova, A.T. Akilbekov, E.A. Kotomin, and S. Piskunov**, "First-principles calculations of defects in MgF₂." – Abstract: PO-146.

27. **A. Usseinov, E.A. Kotomin, Yu.F. Zhukovskii, J. Purans, A. Sorokin, and A.T. Akilbekov**, "First-principles calculations of ZnO crystals doped with hydrogen." – Abstract: PO-168.

28. **A. Sorokin, D. Gryaznov, E.A. Kotomin, and J. Purans**, "First-principles calculations of electronic structure and phonon properties of Al- and H-doped ZnO." – Abstract: PO-169.

29. **A.I. Popov, L. Shirmane, V. Pankratov, V. Dimza, M. Antonova, M. Livinsh, A. Kotlov, and J. Zimmermann**, "VUV synchrotron radiation of PLZT ceramics." – Abstract: PO-176.

VI. 2013 MRS Spring Meeting (San Francisco, USA, April, 2013).

30. **E.A. Kotomin, R. Merkle, Yu.A. Mastrikov, M.M. Kuklja, D. Fuks, and J. Maier**, "Ab initio

modeling of oxygen transport in mixed conducting perovskites for SOFC applications." - Abstract: G6.02.

31. **E.A. Kotomin**, E. Blokhin, **D. Gryaznov**, R.A. Evarestov, and J. Maier, "Ab initio study of confinement effects for ionic carriers in perovskite ultrathin films." - Abstract: XX1.05.

VII. International Conference NANOMEETING-2013 (Minsk, Belarus, May, 2013).

32. **S. Piskunov**, **J. Kazerovskis**, **Yu.F. Zhukovskii**, P.N. Dyachkov, and S. Bellucci, "Incorporation of Ni nanofilament inside carbon nanotubes: DFT calculations."

33. **Yu.N. Shunin**, **Yu.F. Zhukovskii**, V.I. Gopeyenko, N. Burlutskaya, T. Lobanova-Shunina, and S. Bellucci, "Electromagnetic properties of CNTs and GNRs based nanostructures for nanosensor systems."

34. **Yu.F. Zhukovskii**, **S. Piskunov**, **O. Lisovski**, and **J. Begens**, "First principles simulations on doped TiO₂ and SrTiO₃ nanotubular photocatalysts for water-splitting hydrogen generation."

VIII. E-MRS 2013 Spring Meeting (Strasbourg, France, May, 2013).

35. **E.A. Kotomin**, M.M. Kuklja, D. Fuks, **Yu.A. Mastrikov**, O. Sharia, and J. Maier, "Understanding structural stability of complex perovskites for solid oxide fuel cells: First principles calculations." - Abstract: F.P2-1.

36. **E.A. Kotomin**, **D. Bocharov**, **D. Gryaznov**, and **Yu.F. Zhukovskii**, "Ab initio simulations of oxygen interaction with surfaces, interfaces and grain boundaries in uranium mononitride nuclear fuels." - Abstract: M.7-2.

37. **G. Zvejnieks**, **V.N. Kuzovkov**, and **E.A. Kotomin**, "Characterization of self-assembled charged nanoparticle structures." - Abstract: N.P1-9.

38. **V.N. Kuzovkov**, **G. Zvejnieks**, and **E.A. Kotomin**, "Non-equilibrium charge screening in pattern formation kinetics for oppositely charged nanoparticles." - Abstract: N.P1-10.

39. **D. Gryaznov**, **E.A. Kotomin**, E. Blokhin, R.A. Evarestov, J. Maier, and J. Purans, "A comparative ab initio thermodynamic study of oxygen vacancies in oxides." - Abstract: O.P2-5.

40. A. Usseinov, **E.A. Kotomin**, **Yu.F. Zhukovskii**, J. Purans, **A. Sorokin**, and A.T. Akilbekov, "Atomic and electronic structure of hydrogen-doped ZnO: Ab initio hybrid calculations." - Abstract: O.P2-6.

IX. Work Package Meeting of the EC COST project CM 1104 "Reducible oxides" (London, UK, May, 2013).

41. **E.A. Kotomin** and **Yu.A. Mastrikov**, "Ab initio modelling of oxygen transport in (Ba,Sr)(Co,Fe)O₃ perovskite solid solutions for solid oxide fuel cells." - Abstract: p. 1.

42. **Yu.A. Mastrikov** and **E.A. Kotomin**, "Ab initio modeling of oxygen reduction and diffusion in perovskite solid solutions for SOFC and permeation membranes." - Abstract: p. 3.

X. Bunsentagung 2013 Meeting [Annual meeting of German Physical Chemistry Society] (Karlsruhe, Germany, May, 2013).

43. R. Merkle, **Yu.A. Mastrikov**, **E.A. Kotomin**, M.M. Kuklja, and J. Maier, "Comparative analysis of oxygen mobility in (La,Sr)(Co,Fe)O₃ perovskites based on ab initio modeling."

XI. International Symposium on Recent Electronic-Structure Theories and Related Experiments (Stuttgart, Germany, June, 2013).

44. D. Gryaznov, E.A. Kotomin, A. Bussmann-Holder, and J. Maier, "A comparative ab initio thermodynamic study of oxygen vacancies in oxide perovskites: role of phonons."

45. E.A. Kotomin, Yu.A. Mastrikov, R. Merkle, and J. Maier, "A comparative analysis of oxygen vacancy diffusion in LSCF and BSCF perovskite solid solutions: ab initio modeling."

XII. International Symposium on Solid State Ionics (SSI-19) (Kyoto, Japan, June, 2013)

46. M.M. Kuklja, Yu.A. Mastrikov, R. Merkle, E.A. Kotomin, and J. Maier, "Comparative analysis of oxygen mobility in LSCF." - Abstracts: A2-08.

47. R. Merkle, L. Wang, A. Wedig, Yu.A. Mastrikov, E.A. Kotomin, and J. Maier, "Oxygen exchange kinetics on SOFC cathode materials - reaction mechanism and importance of defects." - Abstract: C1-12.

XIII. Annual Monitory Meeting of European Fusion Development Agreement, EFDA - 2013 (Bucharest, Romania, June, 2013).

48. Yu.A. Mastrikov, P.V. Vladimirov, V.A. Borodin, Yu.F. Zhukovskii, E.A. Kotomin, and A. Möslang, "Ab initio modeling of nY/nV_{Fe} complexes diffusion in the α -Fe lattice."

XIV. 25th Joint Russian-German Workshop on ECRH and Gyrotrons (Karlsruhe, Germany, June, 2013).

49. O. Dumbrajs, "Effect of electron beam misalignments on the gyrotron efficiency".

XV. 17th International Conference on Radiation Effects in Insulators, REI'17 (Helsinki, Finland, July, 2013).

50. M.M. Kuklja, E.A. Kotomin, O. Sharia, Yu.A. Mastrikov, and J. Maier, "Radiation defects in complex solid solutions." - Abstract: O-33.

51. F.U. Abuova, A.T. Akilbekov, E.A. Kotomin, S. Piskunov, and V.M. Lisitsyn, "Ab initio modelling of radiation damage in MgF₂." - Abstract: PB-13.

52. D. Gryaznov, E.A. Kotomin, E. Blokhin, R.A. Evarestov, J. Maier, and J. Purans, "A comparative ab initio thermodynamic study of oxygen vacancies in oxides." - Abstract: PB-18.

XVI. European Physical Society Plasma Physics conference (Espoo, Finland, July, 2013).

53. O. Dumbrajs, "RMP ELM suppression analysis by means of a low-dimensional model system for quasi-periodic plasma perturbations".

XVII. Workshop on New Horizons in Electrochemistry- at the Boundary to Physics and Materials Science (Capri, Italy, August, 2013).

54. **E.A. Kotomin, Yu.A. Mastrikov, R. Merkle, and J. Maier**, "Ab initio modelling of oxygen reduction and transport in perovskites for solid oxide fuel cells." - Abstract: p. 24.

XVIII. Advances in the Chemistry of Disordered Solids: Workshop Honouring the Contributions of Professor Patrick Jacobs to Solid State Chemistry (London, UK, September, 2013).

55. **E.A. Kotomin**, "First principles modelling of strongly non-stoichiometric perovskite solid solutions."

XIX. 246th American Chemical Society National Meeting & Exposition (Indianapolis, USA, September, 2013).

56. **M. Kuklja, E.A. Kotomin, D. Fuks, Yu.A. Mastrikov, O. Sharia, R. Merkle, and J. Maier**, "First principles modeling of complex perovskites for energy applications." Abstracts: p. 416.

XX. European Congress on Advanced Materials and Processes, EUROMAT 2013 (Sevilla, Spain, September, 2013).

57. **D. Fuks, M.M. Kuklja, Yu.A. Mastrikov, and E.A. Kotomin**, "Phase stability versus decomposition in complex perovskite solid solutions from DFT study." Symposium E1.III. Materials for Fuel Cells.

XXI. 38th International Conference on Infrared, Millimeter and Terahertz Waves, IRMMW-THz 2013 (Mainz, Germany, September, 2013).

58. **O. Dumbrajs**, "Effect of the tilt on the gyrotron operation". Abstracts: We5-5.

XXII. Ab initio Modelling in Solid State Chemistry, MSSC2013 (London, UK, September, 2013).

59. **P. Zhgun, D. Bocharov, S. Piskunov, A. Kuzmin, and J. Purans**, "Quantum chemistry calculations on negative thermal expansion in scandium fluoride".

XXIII. 14th International Workshop on Nanoscience and Nanotechnology, n&n-2013 (Frascati, Italy, September-October, 2013).

60. **S. Piskunov, Yu.F. Zhukovskii, O. Lisovski, J. Begens, E. Spohr, and S. Bellucci**, "C-, N-, S-, and Fe-doped TiO₂ and SrTiO₃ nanotubes for photocatalytical water-splitting: Prediction from first principles." - Abstracts: p. 15-17.

61. **Yu.N. Shunin, Yu.F. Zhukovskii, V.I. Gopeyenko, N. Burlutskaya, T. Lobanova-Shunina, and S. Bellucci**, "Nanocarbon electromagnetics in CNT-, GNR - and aerogel-based nanodevices." - Abstracts: p. 22-24.

62. **Yu.F. Zhukovskii and R.A. Evarestov**, "Theoretical description of TiO₂ nanowires modeled from densely-packed rutile surfaces." - Abstracts: p. 88-91.

XXIV. 6th International Conference "Physics of Disordered Systems" (Lviv, Ukraine, October, 2013).

63. A. Usseinov, E.A. Kotomin, Yu.F. Zhukovskii, J. Purans, A.T. Akilbekov, and A.K. Dauletbekova, "Hydrogen adsorption on non-polar surfaces of ZnO: Ab initio calculations." - Abstracts: p. 91.

XXV. 2nd General COST Meeting, Action CM 1104 "Reducible Oxide Chemistry" (Uppsala, Sweden, November, 2013).

64. Yu.A. Mastrikov and E.A. Kotomin, "First principles modeling of processes in complex perovskites for solid oxide fuel cells". - Abstracts, p. 67.

XXVI. 6th International Conference on Innovative Information Technologies, IIT-2013 (Vilnius, Lithuania, November, 2013).

65. Yu.N. Shunin, Yu.F. Zhukovskii, V.I. Gopeyenko, T. Lobanova-Shunina, N. Burlutskaya, and S. Bellucci, "Carbon based nanosensor systems for intelligent systems: Modeling and technology."